Scientific Research Publishing

Open Journal of Geology, 2025, 15(11), 788-808
https://www.scirp.org/journal/ojg
ISSN Online: 2161-7589
ISSN Print: 2161-7570

Study on the Control Mechanism of Water-Resisting Performance in Deep High-Pressure Floor Strata

Yang Liu, Qimeng Liu, Zitao Wang, Shuangshuang Hu

School of Earth and Environment, Anhui University of Science and Technology, Huainan, China
Email: 2475133960@qq.com

How to cite this paper: Liu, Y., Liu, Q.M., Wang, Z.T. and Hu, S.S. (2025) Study on the Control Mechanism of Water-Resisting Performance in Deep High-Pressure Floor Strata. *Open Journal of Geology*, **15**, 788-808.
https://doi.org/10.4236/ojg.2025.1511041

Received: October 21, 2025
Accepted: November 24, 2025
Published: November 27, 2025

Abstract

As shallow coal resources become increasingly depleted, deep mining has emerged as an inevitable trend. However, floor water inrush disasters seriously restrict the safe and efficient exploitation of deep coal resources. The traditional water inrush coefficient method has limitations under the conditions of high in-situ stress, high confined water pressure, and strong mining-induced disturbances in deep mining, making it difficult to accurately reflect the hydraulic fracturing and conduits-forming failure mechanism of thick plates. To address this, based on the fluid-solid coupling theory, this study systematically investigates the influence of factors such as lithological combination, effective aquifuge thickness, fault structures, and aquifer water pressure on the failure depth and water-resisting performance of the floor using the FLAC3D numerical simulation method. The results indicate that the lithological combination plays a dominant role in floor stability, with the optimal water-resisting performance observed when the mudstone proportion is approximately 55%. The effective aquifuge thickness shows a positive correlation with the failure depth, but the presence of limestone interlayers exacerbates the failure. Increases in fault conductivity, dip angle, and thickness all significantly deepen the failure zone. For every 1 MPa increase in confined water pressure, the failure zone deepens by an average of 5 - 7 m, identifying water pressure as the key dynamic factor inducing water inrush. This study reveals the instability mechanism of hydraulic fracturing in deep mining floor strata, providing a theoretical basis for the precise prediction and prevention of mine water hazards.

Keywords

Deep Mining, Floor Water Inrush, Fluid-Solid Coupling, Water-Resisting Performance

1. Introduction

With the gradual depletion of shallow coal resources in China, coal mining is expanding into deeper regions. The uncertainty of the geological environment in deep mining increases significantly, among which floor water inrush disasters have become one of the key issues restricting the safe and efficient exploitation of deep coal resources [1]. Conducting research on floor water hazard prevention and control under deep mining conditions is of great practical significance for ensuring the sustainable development of coal resources [2].

Deep mining in North China-type coalfields primarily faces serious threats from the limestone aquifers in the Taiyuan Formation (abbreviated as Taiyuan water) and the Ordovician limestone aquifer (abbreviated as Ordovician water). These aquifers are characterized by highly developed karst fissures. Under the coupled effects of high in-situ stress, high confined water pressure, and strong mining-induced disturbances, the rock mass failure mechanism evolves from the thin plate fracture and instability model used in shallow mining to a thick plate hydraulic fracturing and channeling failure mode dominated by high-pressure water splitting and propagation along fracture networks initiated from mining-induced unloading fractures [3]. This makes deep floor water inrush more concealed and poses severe challenges to existing theories and methods for water inrush risk assessment [4].

The widely used method for water inrush risk assessment at present is the Water Inrush Coefficient Method. This method simplifies the floor as an elastic thin plate bearing uniform water pressure and evaluates the risk by calculating the ratio of water pressure to the equivalent thickness of the aquifuge. As an important part of the theory for mining above confined aquifers, the Water Inrush Coefficient Method plays a positive role in the risk assessment and prediction of coal seam floor water inrush due to its simplicity [5] [6]. However, in the context of deep mining, this method faces certain limitations:

1) The expression of the water inrush coefficient originates from the simplification and approximation of the thin plate fracture theory formula, while deep water inrush is characterized by scattered water gushing, controlled by the thick plate hydraulic fracturing and channeling mechanism. There is a discrepancy between the two mechanical models.

2) Under deep conditions, the balance relationship between the thickness of the floor aquifuge and the confined water pressure exhibits nonlinear characteristics. The linear relationship represented by the water inrush coefficient cannot capture the core physical process of high-pressure hydraulic fracturing.

Therefore, continuing to use the water inrush coefficient to evaluate deep water inrush risk lacks scientific rationality. Taking the Zhuxianzhuang Mine in the Huaibei area as a case study, this paper employs fluid-solid coupling numerical simulation under stress-seepage coupling conditions to investigate the water-resisting performance of the aquifuge under various scenarios. The study aims to deepen the scientific understanding of the instability mechanism of hydraulic

fracturing in deep floor strata and provide theoretical and technical support for the accurate prediction of mine water hazards [7].

2. Methods

Fluid-solid coupling refers to the interaction and feedback mechanism between the groundwater seepage field and the rock mass stress field. That is, changes in fluid pressure lead to adjustments in rock mass stress and deformation, while rock mass deformation, in turn, alters porosity and permeability, thereby affecting fluid movement and pressure distribution [8] [9]. Under deep coal seam mining conditions, the floor strata often simultaneously bear the pressure from the overlying rock mass and the water pressure from the underlying aquifer. The interaction between these two constitutes a typical fluid-solid coupling problem [10].

In an undisturbed state, the floor rock mass is in equilibrium between initial geostress and static water pressure. When mining disturbance occurs, the stress in the floor rock mass redistributes. Local tensile or shear failure causes an increase in pore volume and fracture propagation, significantly increasing the permeability coefficient [11]. This allows the release of confined water energy, causing groundwater to rise along fractures and changing the seepage field. Simultaneously, adjustments in the seepage field act on the rock skeleton through seepage force and pore pressure, causing stress redistribution [12]. If the pore pressure increases and the effective stress decreases, the shear strength of the rock mass declines, making the floor strata more prone to failure and forming connected water channels. This bidirectional interaction between mechanical and hydraulic forces forms a highly nonlinear coupled system, whose evolution directly determines the water-resisting capacity of the floor strata [13].

2.1. Fluid Mass Balance Equation

Finite difference software like FLAC3D is built upon a coupling solution framework based on the Biot equations [14]. Therefore, this study uses FLAC3D as the fluid-solid coupling model builder and solver.

Fluid continuity can be expressed by the volume conservation law as:

$$q_{i,j} + q_v = \frac{\partial \zeta}{\partial t} \tag{1}$$

where, $q_{i,j}$ is the transport velocity of groundwater fluid (m/s), q_v is the source flow intensity of groundwater (1/sec); ζ is the variation in fluid volume or the change in fluid volume per unit volume of porous medium due to fluid diffusion. For saturated media, the volume change is controlled by changes in pore pressure, skeleton deformation, and thermal effects:

$$\frac{\partial \zeta}{\partial t} = \frac{1}{M}\frac{\partial p}{\partial t} + \alpha \frac{\partial \varepsilon}{\partial t} - \beta \frac{\partial T}{\partial t} \tag{2}$$

In the finite difference calculation mode, the change in fluid seepage flow is related to pore pressure p, rock mass volumetric strain ε, and temperature T. In

the above equation, M is the bulk modulus (N/m^2), α represents the influence degree of pore pressure increment on volumetric strain. It indicates the ratio of the fluid volume change in an element to the volume change of the element itself when pore pressure changes, β is the thermal expansion coefficient (1/˚C) considering fluid and solid particles under drained conditions.

When thermal effects can be ignored, the above equation can be simplified to:

$$-q_{i,j} + q_v^* = \frac{1}{M}\frac{\partial p}{\partial t} \tag{3}$$

$$q_v^* = q_v - \alpha\frac{\partial \varepsilon}{\partial t} + \beta\frac{\partial T}{\partial t} \tag{4}$$

2.2. Fluid Motion Equation in Porous Media

Groundwater flow in porous media follows Darcy's law. For homogeneous, isotropic solids and a constant viscosity fluid, Darcy's law can be expressed as:

$$q_i = -k\frac{\partial p}{\partial x_j} - \rho_f g_i \tag{5}$$

where, k is the permeability coefficient of the porous medium (m^2/Pa·s), representing the fluid flow velocity capacity per unit pressure gradient. ρ_f is the fluid density (kg/m^3), g_i (i = 1, 2, 3) are the three components of the gravity vector (m/s^2). The permeability coefficient in FLAC3D differs from the concept in general soil mechanics. The unit of permeability coefficient in FLAC3D is in SI units (m^2/Pa·s), and the conversion relationship with the permeability coefficient k in soil mechanics (cm/s) is:

$$k\left(\mathrm{m}^2/\mathrm{Pa}\cdot\mathrm{s}\right) = k\left(\mathrm{cm/s}\times 1.02\times 10^{-6}\right) \tag{6}$$

2.3. Mechanical Equilibrium Equation and Constitutive Relation

The mechanism of fluid-solid coupling is that after mining, the change in volumetric stress causes a change in the volumetric strain of the rock mass, thereby leading to changes in pore pressure and the permeability of the solid medium; conversely, changes in pore pressure also cause changes in volumetric strain. The equilibrium equation for the solid skeleton of the rock mass can be expressed as:

$$\sigma_{ij,j} + \rho g_i = 0 \tag{7}$$

Considering the influence of pore pressure, the effective stress form is:

$$\sigma'_{ij} = \sigma_{ij} - \alpha p\delta_{ij} \tag{8}$$

Combining this with the linear elastic constitutive relation, the incremental form of the fluid-solid coupling constitutive equation for the porous medium can be obtained:

$$\Delta\sigma_{ij} + \alpha\Delta p\Delta\varepsilon_{ij}^T = H^*\left(\sigma_{ij}, \Delta\varepsilon_{ij} - \Delta\varepsilon_{ij}^T\right) \tag{9}$$

In the formula, $\Delta\sigma_{ij}$ is the stress increment; H^* is a given indicator function; ε_{ij} is the total strain; $\Delta\varepsilon_{ij}^T$ is the Kronecker delta, representing thermal strain.

Furthermore, the relationship between the strain rate and the velocity gradient is:

$$\varepsilon_{ij} = \frac{v_{i,j} + v_{j,i}}{2} \tag{10}$$

In the formula, v_j is the velocity of a point in the medium. Thus, it can be seen that changes in pore pressure directly affect the stress state of the rock mass, thereby altering its stability.

2.4. Coupling Solution Process

The FLAC3D coupling solution process uses an explicit finite difference scheme, advancing the time step through alternating iterations of stress and pore pressure. First, the effective stress and deformation are calculated based on the current pore pressure field; then, the permeability and pore pressure distribution are updated based on the deformation results. Each time step satisfies fluid conservation and mechanical equilibrium until convergence.

This method can capture transient processes such as pore pressure diffusion, fracture connection, and stress release in the floor rock mass under mining disturbance. Its formulation is expressed as:

$$\frac{E}{2(1+v)} u_{i,ij} + \frac{E}{2(1+v)(1-2v)} u_{k,ki} + \alpha p_i = 0 \tag{11}$$

where, u_i is the displacement in the x_i direction, α is the pressure coefficient, $\alpha = 1 - K_s/K_g$, where K_s is the bulk modulus of the porous medium, and K_g is the grain bulk modulus.

2.5. Model Generalization and Boundary Conditions

Taking a working face in the Zhuxianzhuang Mine as an example, a model measuring 600 m in length, 200 m in width, and 220 m in height was established. Additionally, this simulation simulates a mining advance length of 400 m along the strike direction. The model is divided into multiple-layered units, including the coal seam, roof, floor, and underlying aquifer. To eliminate the influence of boundary conditions on the mining disturbance area, 50 m protective coal pillars are reserved at both ends along the working face advance direction.

1) Mechanical Boundary Conditions

The bottom of the model is set as a fully fixed boundary, with displacements and velocities set to 0 in the *x*, *y*, and *z* directions. The side boundaries are set with horizontal constraints. The top of the model is set as a free boundary to simulate surface stress release conditions [15].

2) Seepage Boundary Conditions

The fluid boundaries use a combination of closed and open types. A constant head boundary is applied at the contact surface between the model bottom and the underlying confined aquifer; the contact surface between the model top and the ground surface is a free drainage boundary; all side boundaries of the model are set as impermeable boundaries to ensure water flow primarily propagates vertically.

3) Model Mechanical Parameters

The physical and mechanical parameters of each rock type were determined based on the in-situ measurements from the production geological report of the Zhuxianzhuang Mine, as listed in Table 1.

Table 1. Model mechanical parameters.

	Density (kg/cm^3)	Elastic Mod (GPa)	Poisson's Ratio	Cohesion (MPa)	Tensile Strength (MPa)	Friction Angle (˚)
Siltstone	2.57	3.21	0.27	2.48	2.06	37.9
Limestone	2.90	3.02	0.26	3.40	2.56	43.5
Post stone	2.70	3.103	0.29	2.40	1.29	42.0
Coal #10	1.40	0.50	0.32	1.90	2.50	27.0
Mudstone	2.54	2.13	0.33	2.10	1.74	32.3
Coal Seam	1.40	0.50	0.32	2.60	2.20	27.0

4) Geological Model Schematic

A schematic diagram of the numerical model structure is shown in Figure 1.

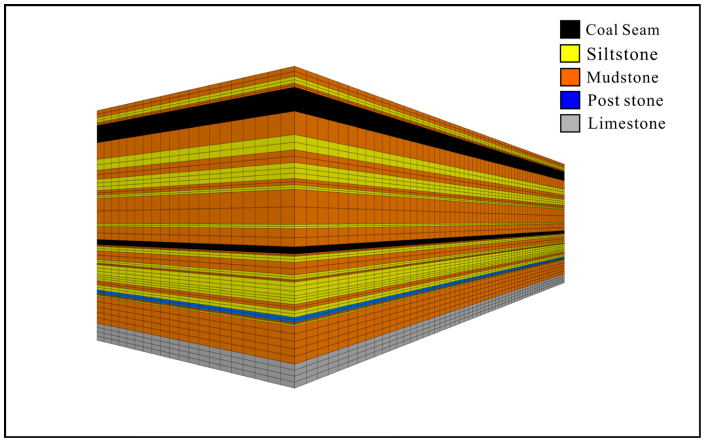

Figure 1. Numerical simulation model.

2.6. Scenario Design for Factors Influencing Floor Water-Resisting Performance

To quantitatively identify the influence degree of various factors, multiple sets of representative geological-hydrological-structural scenarios were constructed to systematically analyze the influence mechanisms of lithological combination, effective aquifuge thickness, fault structures, and aquifer water pressure on the development of the floor failure zone and changes in the water-resisting coefficient. Four basic scenario groups were designed: 1) Lithological combination variation group; 2) Effective aquifuge thickness variation group; 3) Fault structural condition variation group; 4) Confined water pressure variation group.

2.6.1. Lithological Combination Variation Scenario Design

Lithological combination is the most basic geological factor controlling the floor's

water-resisting capacity, as different rock layers have significant differences in physical-mechanical properties and permeability characteristics [16]. To investigate the influence of lithological combinations on the water-resisting capacity of the floor strata, six working conditions were established by varying the thickness proportion of mudstone in the aquifuge, with mudstone proportions set at 0%, 45%, 55%, 65%, 75%, and 100%, respectively. The control variables for this scenario were set as: effective aquifuge thickness 60 m, bottom confined water pressure 3 MPa, no fault structure, mining advance length 400 m, and other parameters consistent with the baseline model.

2.6.2. Effective Aquifuge Thickness Variation Scenario Design

The effective aquifuge thickness is a key parameter in the definition of the water-resisting coefficient, directly determining the ability of the floor strata to resist the rise of confined water and mining disturbances. Under fixed mudstone proportion (55%) and water pressure (3 MPa) conditions, the following four effective aquifuge thickness working conditions were designed: 1) 20 m (excluding limestone layers, thin aquifuge condition); 2) 40 m (medium thickness condition); 3) 60 m (thick aquifuge condition, excluding limestone layers); 4) 60 m (including the first and second limestone layers). The effective aquifuge thickness is a key parameter in the definition of the water-resisting coefficient, directly determining the ability of the floor strata to resist the rise of confined water and mining disturbances. Under fixed mudstone proportion (55%) and water pressure (3 MPa) conditions, the following four effective aquifuge thickness working conditions were designed: 1) 20 m (excluding limestone layers, thin aquifuge condition); 2) 40 m (medium thickness condition); 3) 60 m (thick aquifuge condition, excluding limestone layers); 4) 60 m (including the first and second limestone layers).

2.6.3. Structural Condition Variation Scenario Design

Faults and structural fracture zones are commonly developed in deep mining areas. Their water-conducting capacity and mechanical weakening effects have a decisive influence on the stability of the water-resisting layer [17]. To systematically analyze the multi-dimensional influence of structural characteristics, this study sets working conditions from three aspects: fault water conductivity, dip angle, and thickness.

1) Fault Water Conductivity Type

Faults are divided into three categories: water-conducting fault, weakly water-conducting fault, and non-water-conducting fault. The fault width in the model is set to 10 m, dip angle 45˚, penetrating the middle of the floor and extending to the top boundary of the aquifer.

2) Fault Dip Angle Variation

To analyze the influence of fault dip angle on the development of seepage channels and stress transmission paths, dip angles of 30˚, 45˚, and 60˚ were set, keeping the fault thickness and water conductivity constant (water-conducting fault condition).

3) Fault Thickness Variation

The fault zone thickness reflects the width of the fracture zone and the integrity

of the rock mass. Scenarios with thicknesses of 5 m, 10 m, and 15 m were set up, while keeping other conditions consistent.

For all structural scenarios, other parameters were fixed as: mudstone proportion 60%, effective aquifuge thickness 60 m, water pressure 3 MPa.

2.6.4. Aquifer Water Pressure Variation Scenario Design

Aquifer water pressure is an important controlling factor determining the potential energy of confined water and the risk of water inrush. Its changes directly affect the pore water pressure distribution and effective stress state. To analyze the effect of water pressure intensity on the stability of the water-resisting layer, under fixed lithological combination (mudstone proportion 65%), effective aquifuge thickness (60 m), and no fault conditions, four incrementally increasing water pressure working conditions were designed: 2 MPa, 3 MPa, 4 MPa, and 5 MPa.

3. Results and Discussion

3.1. Analysis of Lithological Combination Scenario Results

Simulation results for different lithological combinations show significant differences in the spatial distribution of the yield failure zone in the floor under these scenarios (Figures 2-7). When the floor is dominated by sandstone (mudstone proportion 0%), the failure zone is extensive and extends deep; when the mudstone proportion is moderate, the failure zone contracts significantly; when the mudstone proportion is too high (>70%) or reaches 100% (entirely mudstone), the failure zone expands again, showing a characteristic of first decreasing and then increasing.

Figure 8 shows the statistical results of floor failure zone depth under different mudstone proportions. When the mudstone proportions are 0%, 45%, 55%, 65%, 75%, and 100%, the floor failure zone depths are 31.29 m, 27.18 m, 20.63 m, 29.14 m, 26.85 m, and 47.21 m, respectively. When the floor is entirely composed of sandstone, the plastic zone develops significantly along the coal seam floor, with a failure zone depth of 31.29 m, and the fracture zone shows a wedge-shaped structure wide at the top and narrow at the bottom. This is because sandstone is dense and brittle, mining stress concentrates near the interface, and local tension easily induces connected fractures. As the mudstone proportion increases to about 45% - 65%, the failure zone contracts significantly, with the plastic zone mainly distributed in the shallow part of the floor, while the deep part remains intact, indicating a significant enhancement in water-resisting capacity. When the mudstone proportion is 55%, the failure zone depth is the smallest, only 20.63 m, and the water-resisting performance is optimal (Figure 8).

However, when the mudstone proportion continues to increase beyond 75%, the floor failure depth increases again. For example, when the mudstone proportion reaches 100%, the failure zone depth increases to 47.21 m, almost penetrating to the top of the limestone layer. The reason is that although mudstone has low permeability, which is beneficial for water resistance, its mechanical strength is weak, and its elastoplastic deformation capacity is limited, making it prone to

shear yielding and interlayer slippage under mining stress, thereby promoting the reformation of seepage channels. This shows that the lithological combination of the floor has a nonlinear optimal range for water-resisting performance. When plastic and brittle layers are interbedded in a certain proportion, they can form a synergistic effect of stress dissipation and seepage obstruction, significantly improving the overall anti-inrush capacity [18].

This indicates that a moderate mudstone proportion not only improves the overall ductility of the floor but also enhances the self-stability and closure capacity of the water-resisting layer. Sandstone acts as the "skeleton" bearing the load, while mudstone functions as the "muscles and ligaments" to dissipate energy and inhibit damage propagation. Any deviation toward a lower mudstone proportion causes the aquifuge to lose its capacity for energy dissipation and damage inhibition, transforming into a brittle system where fractures propagate unimpeded. Conversely, a deviation toward a higher mudstone proportion leads to the loss of the "high-strength skeleton", resulting in a weak system prone to extensive shear flow failure. Therefore, a reasonable lithological combination, especially when the sandstone to mudstone interbedding ratio is about 1:1 to 3:2, can form an optimal water-resisting structure, which is an important reference for the selection and evaluation of water-resisting layers in deep mining areas.

1) Mudstone proportion 0%

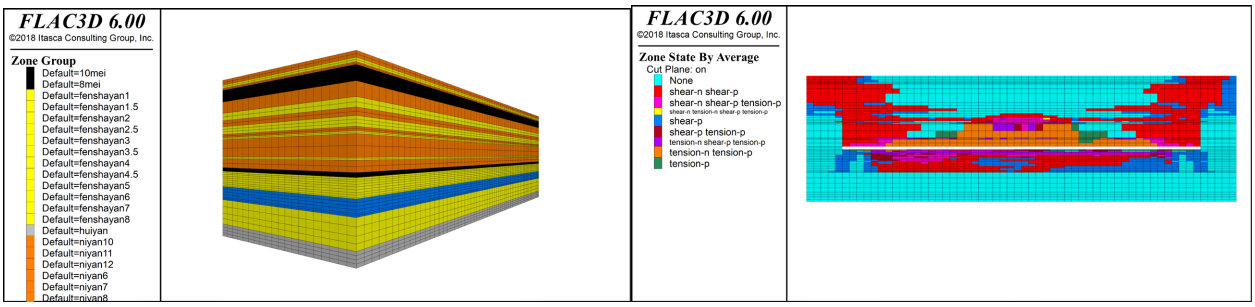

(a) (b)

Figure 2. Simulation results for mudstone proportion 0%: (a) Model diagram; (b) Mining-induced plastic zone.

2) Mudstone proportion 45%

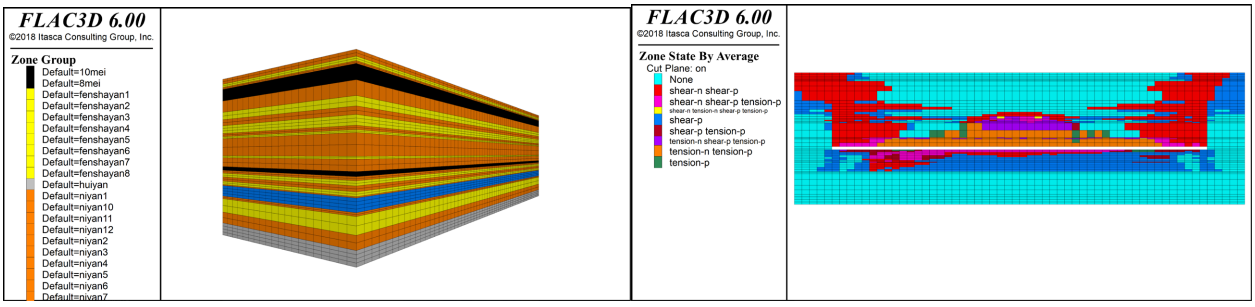

(a) (b)

Figure 3. Simulation results for mudstone proportion 45%: (a) Model diagram; (b) Mining-induced plastic zone.

3) Mudstone proportion 55%

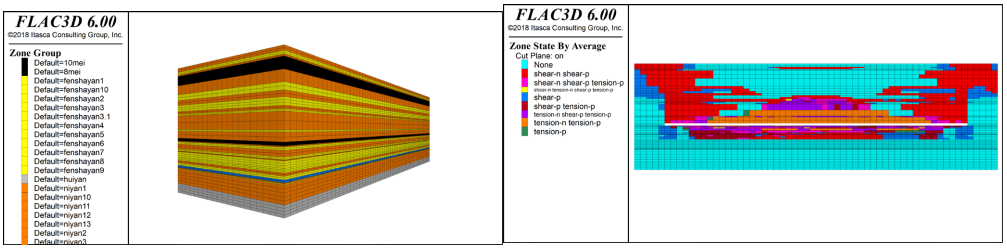

(a) (b)

Figure 4. Simulation results for mudstone proportion 55%: (a) Model diagram; (b) Mining-induced plastic zone.

4) Mudstone proportion 65%

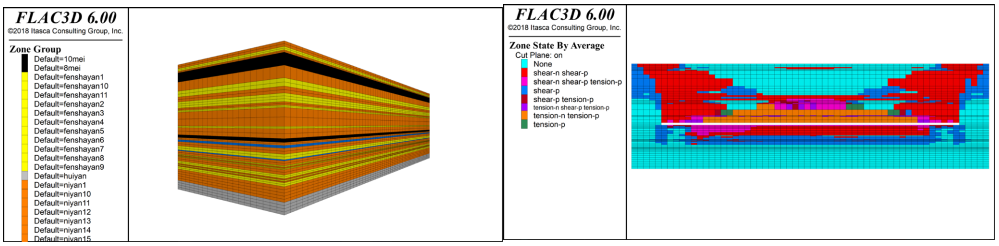

(a) (b)

Figure 5. Simulation results for mudstone proportion 65%: (a) Model diagram; (b) Mining-induced plastic zone.

5) Mudstone proportion 75%

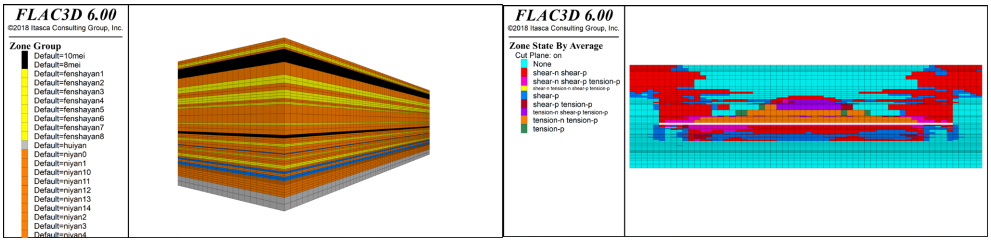

(a) (b)

Figure 6. Simulation results for mudstone proportion 75%: (a) Model diagram; (b) Mining-induced plastic zone.

6) Mudstone proportion 100%

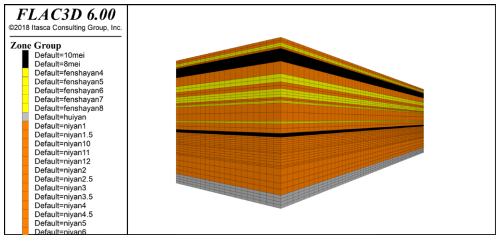

(a)

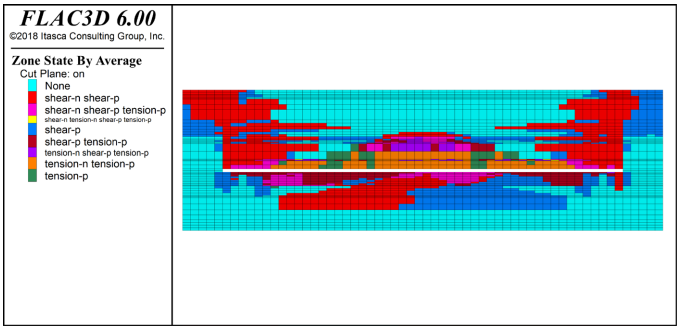

(b)

Figure 7. Simulation results for mudstone proportion 100%: (a) Model diagram; (b) Mining-induced plastic zone.

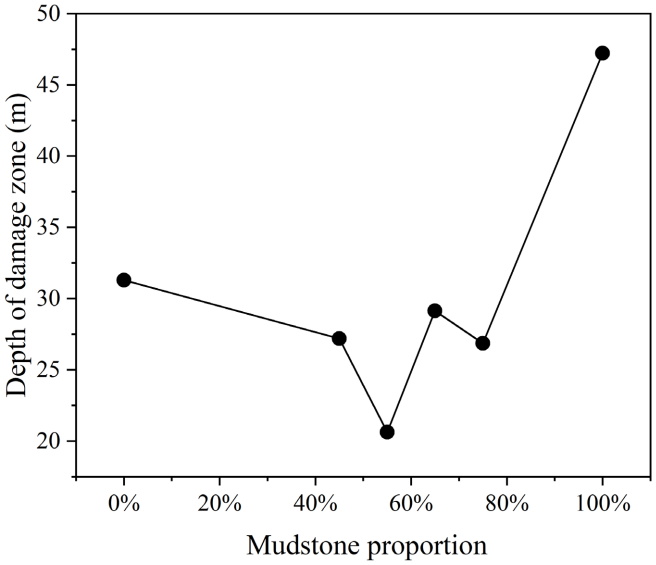

Figure 8. Failure zone depth under different mudstone proportions.

3.2. Analysis of Effective Aquifuge Thickness Variation Scenario Results

The thickness of the effective aquifuge reflects the buffer distance between the confined water and mining-induced disturbances, serving as a crucial control parameter for determining floor water inrush risk. Simulation results (**Figures 9-12**) show that when the effective aquifuge thickness is relatively small (20 m), the failure zone in the floor is limited to local shallow areas, while the deeper limestone layers remain stable. As the thickness increases to 40 m and 60 m, the extent of the failure zone expands, reaching 24.15 m and 27.2 m, respectively. When the first and second limestone layers are included under the same thickness conditions, the failure zone further extends to 30.9 m. Due to their high elastic modulus and brittleness, limestone layers are prone to developing tensile fractures under mining-induced loading, leading to localized stress concentration and forming a hard-brittle layer-induced failure mode.

This indicates a critical-effect relationship between aquifuge thickness and wa-

ter-resisting performance: if the layer is too thin, it is easily penetrated directly by mining disturbances; if too thick, new fracture channels may form due to differential interlayer strain.

1) Effective aquifuge thickness 20 m (excluding the first and second limestone layers)

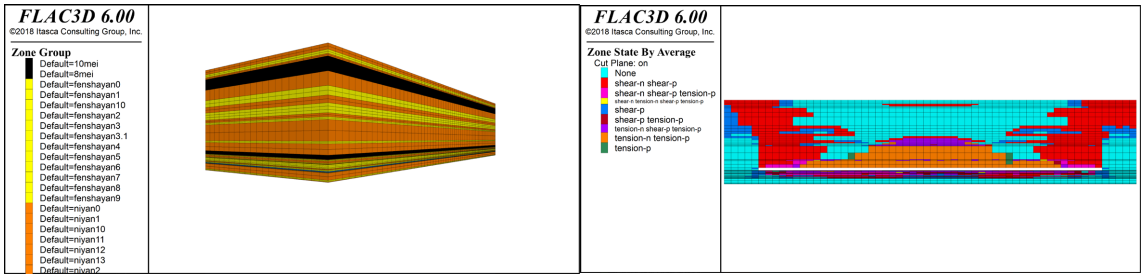

(a) (b)

Figure 9. Simulation results for effective aquifuge thickness 20 m (excluding limestone layers): (a) Model diagram; (b) Mining-induced plastic zone.

2) Effective aquifuge thickness 40 m (excluding the first and second limestone layers)

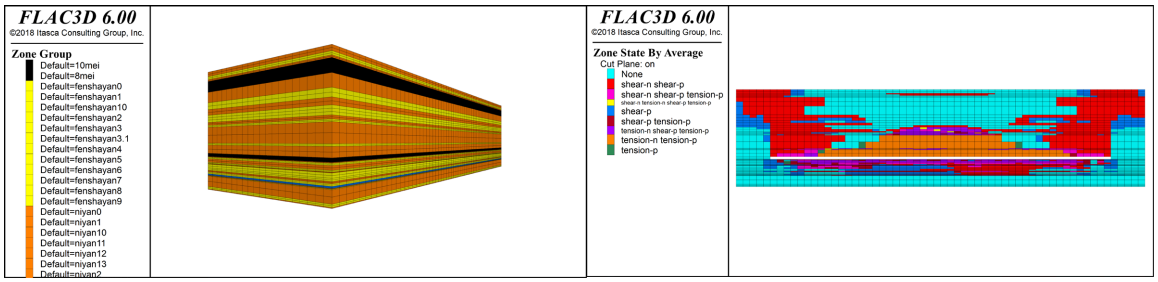

(a) (b)

Figure 10. Simulation results for effective aquifuge thickness 40 m (excluding limestone layers): (a) Model diagram; (b) Mining-induced plastic zone.

3) Effective aquifuge thickness 60 m (excluding the first and second limestone layers)

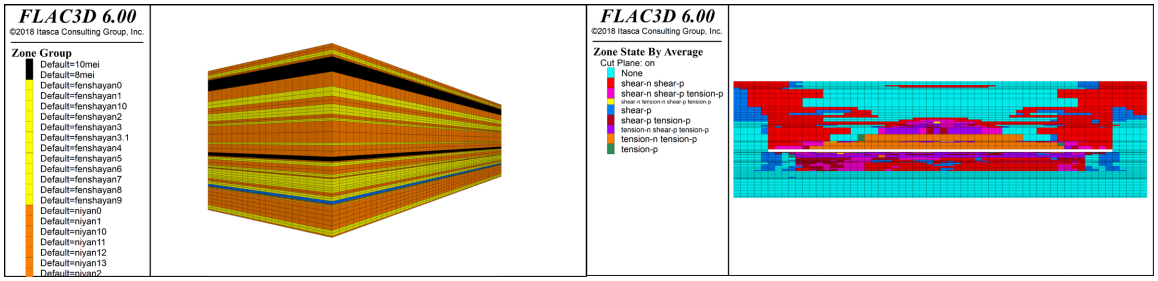

(a) (b)

Figure 11. Simulation results for effective aquifuge thickness 60 m (excluding limestone layers): (a) Model diagram; (b) Mining-induced plastic zone.

4) Effective aquifuge thickness 60 m (including the first and second limestone layers)

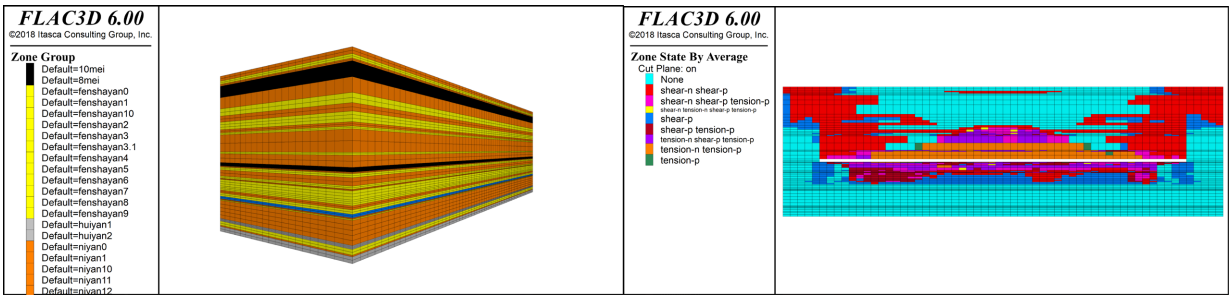

(a) (b)

Figure 12. Simulation results for effective aquifuge thickness 60 m (including limestone layers): (a) Model diagram; (b) Mining-induced plastic zone.

3.3. Analysis of Structural Condition Variation Scenario Results

Structural factors, especially the development state of faults, are key geological conditions affecting the stability of the deep floor and the evolution of water hazards. Faults not only alter the local stress field distribution but can also act as seepage channels, directly determining the possibility of confined water seeping into the goaf [19]. Through fluid-solid coupling simulation, the influence patterns of fault water conductivity, dip angle, and thickness on floor failure were systematically analyzed.

1) Influence of Fault Water Conductivity

Comparison results of three typical scenarios (water-conducting fault, weakly water-conducting fault, non-water-conducting fault) show (**Figures 13-15**) that enhanced fault water conductivity significantly aggravates plastic failure in the floor. The failure zone depths are 21.32 m, 23.09 m, and 24.64 m, respectively, showing a stepwise increasing trend with enhanced water conductivity. This indicates that the stronger the water-conducting capacity of the fault, the easier it is to form a dominant seepage channel for high-pressure water flow under mining influence, leading to significant extension of the failure zone to deeper parts.

1) Water-conducting fault

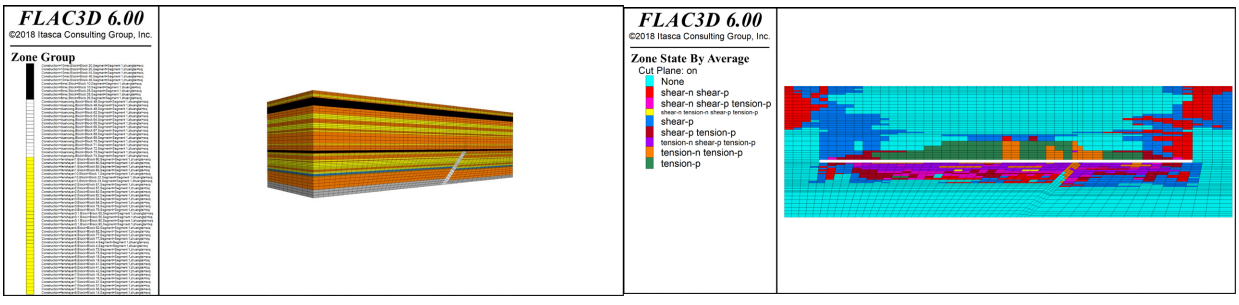

(a) (b)

Figure 13. Simulation results with water-conducting fault: (a) Model diagram; (b) Mining-induced plastic zone.

2) Weakly water-conducting fault

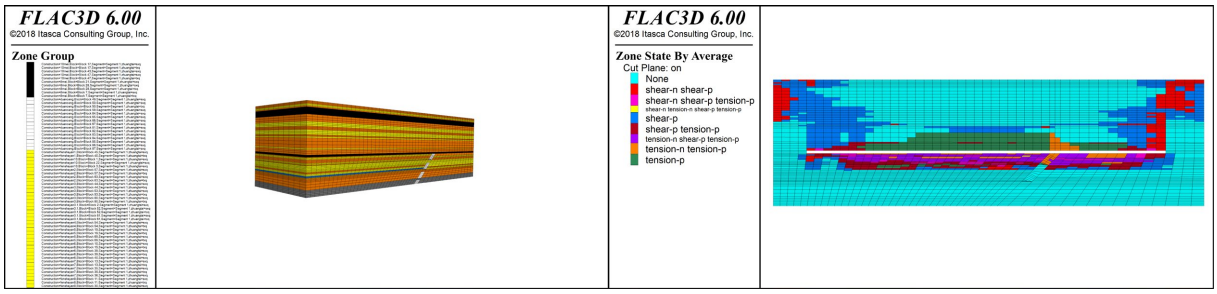

(a) (b)

Figure 14. Simulation results with weakly water-conducting fault: (a) Model diagram; (b) Mining-induced plastic zone.

3) Non-water-conducting fault

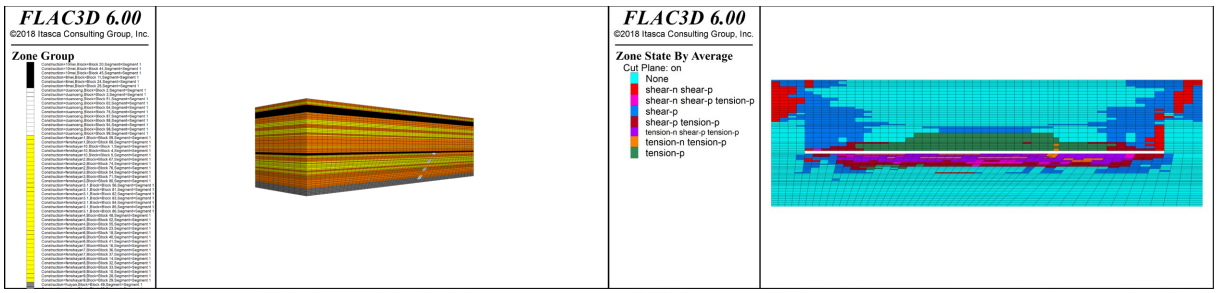

(a) (b)

Figure 15. Simulation results with non-water-conducting fault: (a) Model diagram; (b) Mining-induced plastic zone.

2) Influence of Fault Dip Angle (Taking Water-conducting Fault as an Example)

When the fault is water-conducting, the change in dip angle has a noticeable impact on floor stability. As the dip angle increases from 30˚ to 60˚, the failure zone depth increases from 23.65 m to 26.26 m (**Figures 16-18**). This indicates that steeper dip angle faults promote the extension of mining influence to deeper parts of the strata, exacerbating plastic failure in the floor rock mass. An increase in dip angle reduces the angle between the fault strike and the principal stress direction, making stress concentration more easily diffuse along the fault plane, forming deep seepage channels [20].

1) Dip angle 30˚

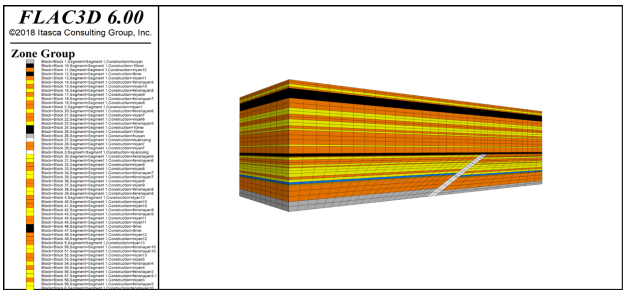

(a)

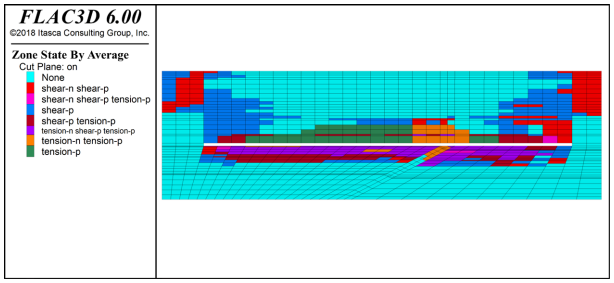

(b)

Figure 16. Simulation results with 30˚ water-conducting fault: (a) Model diagram; (b) Mining-induced plastic zone.

2) Dip angle 45˚

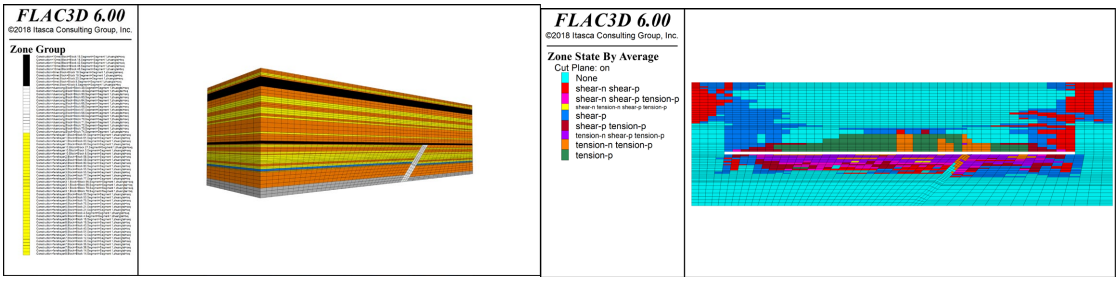

(a) (b)

Figure 17. Simulation results with 45˚ water-conducting fault: (a) Model diagram; (b) Mining-induced plastic zone.

3) Dip angle 60˚

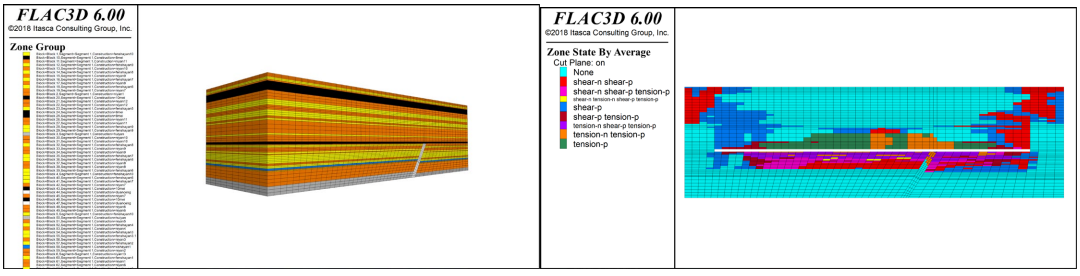

(a) (b)

Figure 18. Simulation results with 60˚ water-conducting fault: (a) Model diagram; (b) Mining-induced plastic zone.

Fault thickness also shows a positive correlation. When the thickness increases from 5 m to 15 m, the failure zone depth increases from 22.77 m to 26.21 m (**Figures 19-21**). The infill material inside thick faults is mostly argillaceous cataclasite or brecciated structure, with significantly degraded mechanical properties, making it prone to compression-shear failure and forming connected zones under mining disturbance. Simultaneously, thick faults provide a larger volume for seepage channels, enhancing the upward seepage capacity of confined water.

1) Thickness 5 m

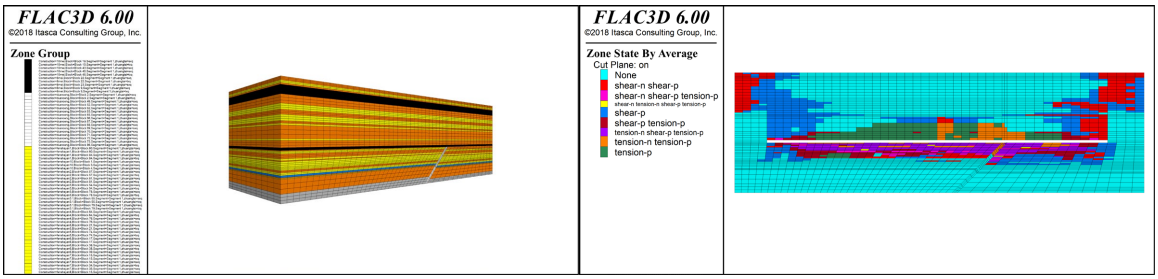

(a) (b)

Figure 19. Simulation results with 5 m water-conducting fault: (a) Model diagram; (b) Mining-induced plastic zone.

2) Thickness 10 m

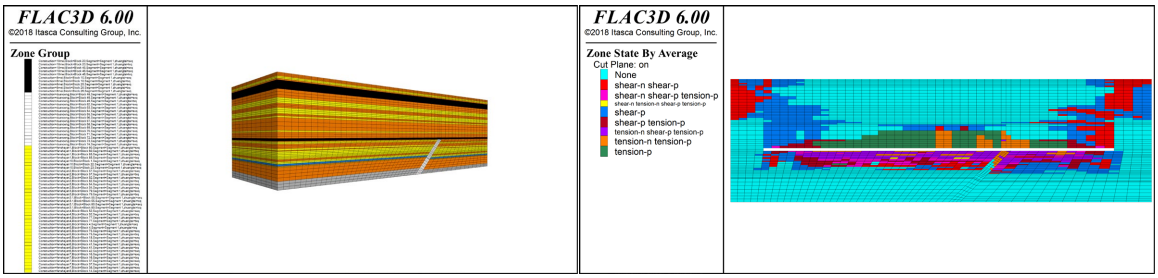

(a) (b)

Figure 20. Simulation results with 10 m water-conducting fault: (a) Model diagram; (b) Mining-induced plastic zone.

3) Thickness 15 m

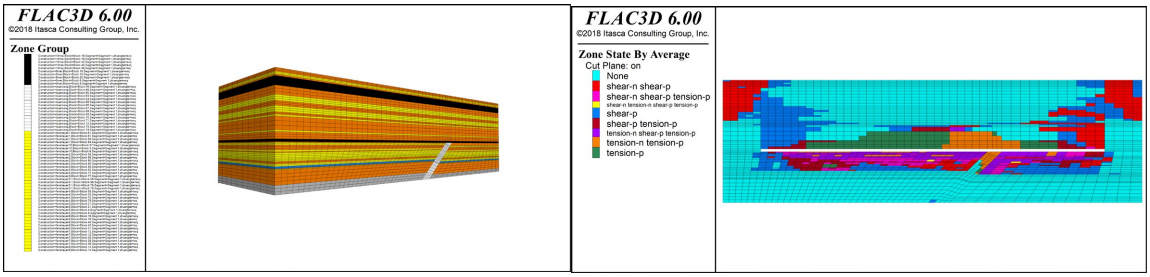

(a) (b)

Figure 21. Simulation results with 15 m water-conducting fault: (a) Model diagram; (b) Mining-induced plastic zone.

In summary, the water conductivity, dip angle, and thickness of faults collectively determine the degree to which they compromise the integrity of the water-resisting layer. More developed water-conducting faults, steeper dip angles, and greater thicknesses lead to deeper failure zones in the floor and a significant increase in water inrush risk.

3.4. Analysis of Aquifer Water Pressure Variation Scenarios

The confined water pressure is the direct driving force behind water inrush disas-

ters, and its magnitude determines the stress state and failure mode of the floor aquifuge. Numerical simulations under different water pressure conditions (Figures 22-25) show that the depth of the floor failure zone increases continuously with rising water pressure. Specifically, when the water pressures are 2 MPa, 3 MPa, 4 MPa, and 5 MPa, the failure zone depths are 21.72 m, 29.14 m, 35.50 m, and 39.05 m, respectively (Figure 26).

The study indicates that the weakening effect of increasing water pressure on floor stability is primarily manifested in two aspects. On one hand, according to Terzaghi's principle, an increase in pore water pressure directly reduces the effective stress in the rock mass, significantly decreasing its shear and tensile strengths. Under high water pressure conditions, micro-fractures within the rock mass open more easily, porosity increases, and permeability is consequently enhanced, further promoting water flow ascent and pore pressure diffusion, creating a failure amplification effect. On the other hand, when the pore pressure exceeds the tensile strength of the rock mass, it induces hydraulic fracturing, generating new seepage channels. Particularly at the interface between limestone and sandstone, due to the abrupt change in lithology and significant difference in elastic modulus, these areas easily become stress concentration zones and initiation points for fracturing. The propagation of hydraulic fractures not only weakens local strength but may also cause a breakthrough in the aquifuge, forming stable seepage pathways.

1) Water Pressure 2 MPa

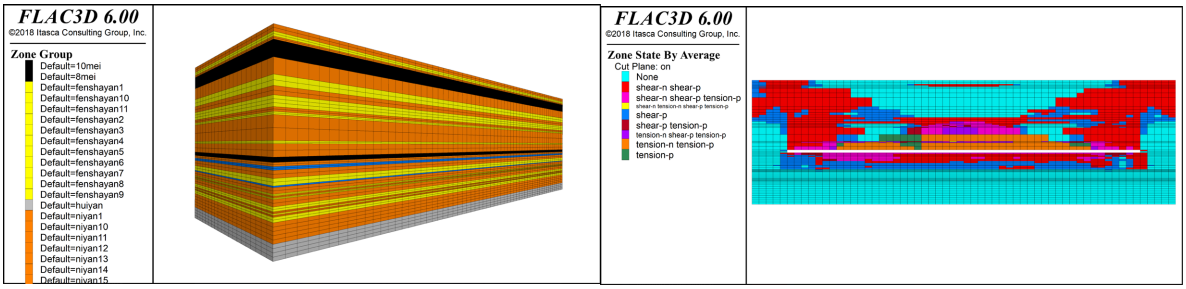

(a) (b)

Figure 22. Simulation results under 2 MPa water pressure: (a) Model diagram; (b) Mining-induced plastic zone.

2) Water Pressure 3 MPa

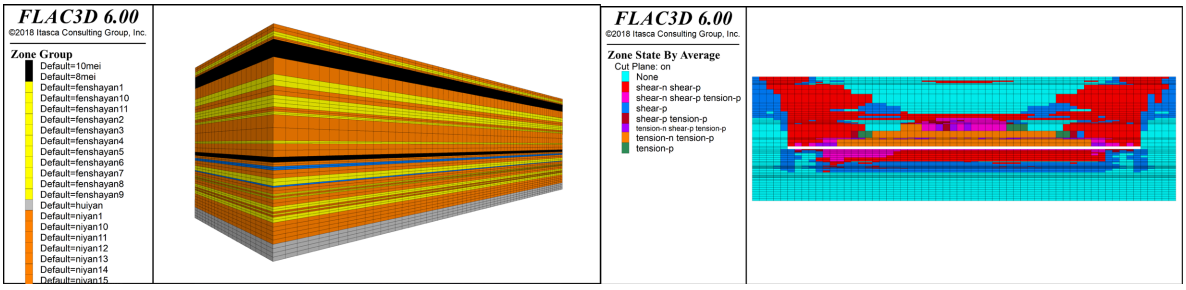

(a) (b)

Figure 23. Simulation results under 3 MPa water pressure: (a) Model diagram; (b) Mining-induced plastic zone.

3) Water Pressure 4 MPa

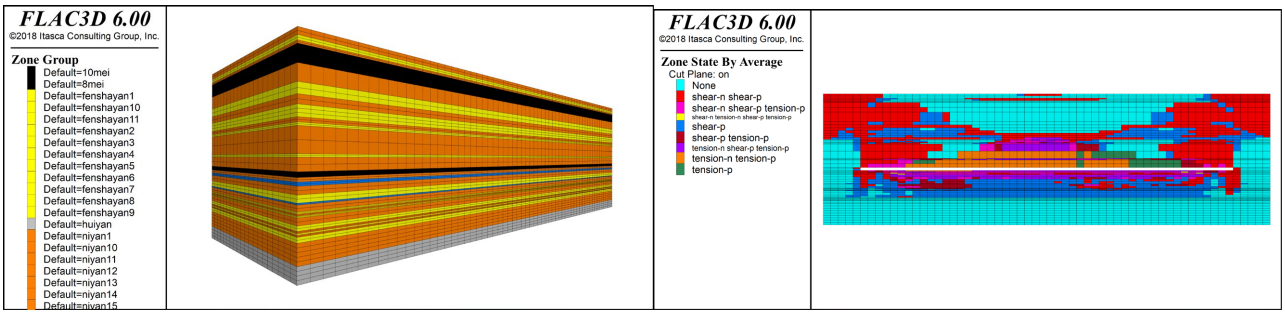

(a) (b)

Figure 24. Simulation results under 4 MPa water pressure: (a) Model diagram; (b) Mining-induced plastic zone.

4) Water Pressure 5 MPa

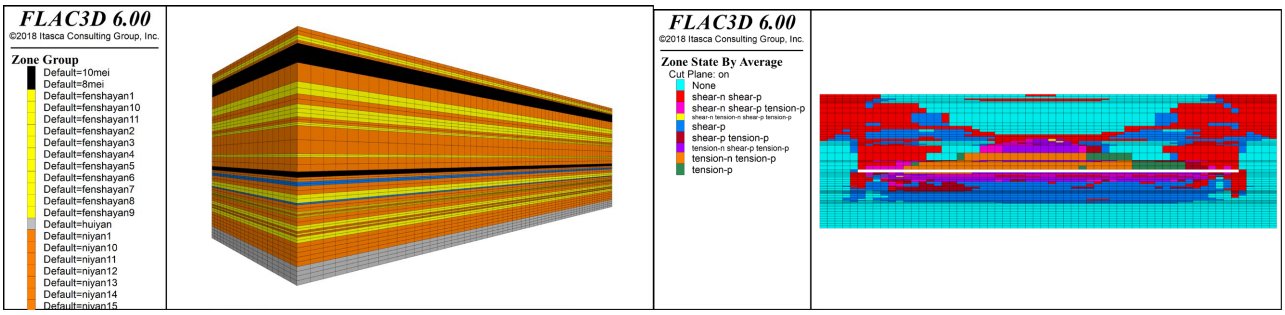

(a) (b)

Figure 25. Simulation results under 5 MPa water pressure: (a) Model diagram; (b) Mining-induced plastic zone.

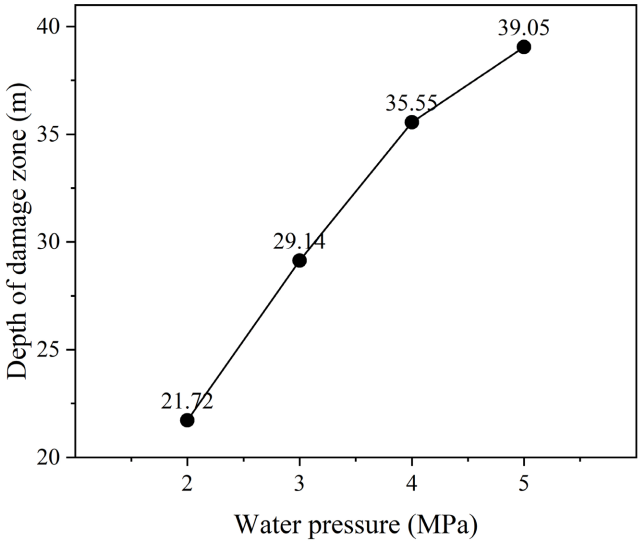

Figure 26. Failure zone depth under different water pressures.

The numerical results indicate that for every 1 MPa increase in water pressure, the floor failure zone deepens by approximately 5 m to 7 m on average, demon-

strating the high sensitivity of the water-resisting coefficient to water pressure.

4. Conclusions

Based on fluid-solid coupling theory, the FLAC3D numerical simulation method was used to systematically study the control mechanisms of different geological and hydrogeological factors on the floor failure depth and water-resisting performance. The research results indicate:

1) Lithological combination is the main controlling factor affecting the floor's water-resisting performance. The elastoplastic and permeability characteristics of different rock layer types determine the overall stability of the floor. When the mudstone proportion is about 55%, the floor failure depth is minimal (20.63 m), and the water-resisting performance is optimal; a moderate proportion of mudstone layers enhances the integrity of the composite rock strata through strain energy absorption and fracture passivation. When the mudstone proportion is too low or too high, the structural stability of the floor decreases, and failure intensifies, especially under a single mudstone condition (100%), where the failure depth reaches 47.21 m, indicating that lithological combination is crucial for maintaining the structural toughness of the water-resisting layer.

2) The effective aquifuge thickness has a dual influence on floor failure. Simulation results show that the failure depth increases from 12.02 m to 27.2 m as the aquifuge thickness increases from 20 m to 60 m, showing a positive correlation; under the same thickness condition, if limestone layers are included, the failure depth further increases to 30.9 m. The high stiffness and brittleness of limestone lead to significant stress concentration effects, causing the plastic zone to extend deeper. This indicates that while a greater aquifuge thickness enhances the capacity to isolate confined water, significant differences in internal lithology may also induce the development of secondary fractures.

3) Structural factors have an amplifying effect on floor failure. Water conductivity, dip angle, and thickness collectively determine the degree of failure in the fault zone and the characteristics of seepage channel development. The failure zone under water-conducting fault conditions is significantly deeper and more prone to forming seepage channels compared to non-water-conducting faults; when the dip angle increases from 30˚ to 60˚, the failure depth increases from 23.65 m to 26.26 m; when the thickness increases from 5 m to 15 m, the failure depth increases from 22.77 m to 26.21 m. This shows that larger fault scale, steeper dip angle, and stronger water conductivity lead to more significant weakening of the floor aquifuge integrity.

4) Confined water pressure is a key external factor controlling floor stability. As the water pressure increases from 2 MPa to 5 MPa, the floor failure depth increases from 21.72 m to 39.05 m. High water pressure significantly enhances the permeability and instability tendency of the floor rock mass by reducing effective stress, promoting fracture opening, and inducing hydraulic fracturing, making it the direct dynamic factor for water inrush disasters.

Conflicts of Interest

The authors declare no conflicts of interest regarding the publication of this paper.

References

[1] Gu, Q., Huang, Z., Li, S., Zeng, W., Wu, Y. and Zhao, K. (2020) An Approach for Water-Inrush Risk Assessment of Deep Coal Seam Mining: A Case Study in Xinlongzhuang Coal Mine. *Environmental Science and Pollution Research*, **27**, 43163-43176. https://doi.org/10.1007/s11356-020-10225-0

[2] Shi, L., Qu, X., Yu, X., Li, Y., Pei, F., Qiu, M., *et al.* (2020) Theory and Practice on the Division of the "Water Pressure-Free Zone" in a Mining Coal Seam Floor. *Arabian Journal of Geosciences*, **13**, Article No. 1079. https://doi.org/10.1007/s12517-020-06067-2

[3] Sun, M., Guo, C., Zheng, W. and Duan, H. (2021) Study on Broken Floor Rock Mass by Mining Underground Pressure. *Mathematical Problems in Engineering*, **2021**, Article ID: 3797188. https://doi.org/10.1155/2021/3797188

[4] Li, A., Ding, X., Yu, Z., Wang, M., Mu, Q., Dai, Z., *et al.* (2022) Prediction Model of Fracture Depth and Water Inrush Risk Zoning in Deep Mining Coal Seam Floor. *Environmental Earth Sciences*, **81**, Article No. 315. https://doi.org/10.1007/s12665-022-10431-8

[5] Liu, Y., Liu, S., Huo, Z., Sun, K., Wang, T. and Li, W. (2022) Failure Characteristics of Coal Seam Floor and Risk Assessment of Water Inrush Caused by Underground Coal Mining. *Energy Exploration & Exploitation*, **41**, 677-695. https://doi.org/10.1177/01445987221144332

[6] Duan, H. and Zhao, L. (2021) New Evaluation and Prediction Method to Determine the Risk of Water Inrush from Mining Coal Seam Floor. *Environmental Earth Sciences*, **80**, Article No. 30. https://doi.org/10.1007/s12665-020-09339-y

[7] Wang, X. (2021) Frack Evolution and Destruction Characteristics of Mining Bottom Plate on Pressurized Water Based on Similar Simulation. *Geotechnical and Geological Engineering*, **40**, 1499-1511. https://doi.org/10.1007/s10706-021-01980-z

[8] Li, W., Liu, Y., Li, S., Ma, L., Yue, L. and Wang, J. (2024) Experimental and Numerical Studies of Water-Sand Flow in Fractured Porous Media. *Rock Mechanics and Rock Engineering*, **57**, 6485-6509. https://doi.org/10.1007/s00603-024-03862-1

[9] Wu, W. and Wang, Z. (2021) Numerical Simulation of Fluid-Solid Coupling of Stress Failure Characteristics of Floor in Coal Mining Face. *IOP Conference Series: Earth and Environmental Science*, **766**, Article ID: 012017. https://doi.org/10.1088/1755-1315/766/1/012017

[10] Tang, C.A., Tham, L.G., Lee, P.K.K., Yang, T.H. and Li, L.C. (2002) Coupled Analysis of Flow, Stress and Damage (FSD) in Rock Failure. *International Journal of Rock Mechanics and Mining Sciences*, **39**, 477-489. https://doi.org/10.1016/s1365-1609(02)00023-0

[11] Li, Z., Wang, L., Ding, K., Ren, B., Wang, S., Jiang, C., *et al.* (2022) Study on Fracture and Seepage Evolution Law of Stope Covered by Thin Bedrock under Mining Influence. *Minerals*, **12**, Article 375. https://doi.org/10.3390/min12030375

[12] He, T., Li, G., Sun, C., Luo, F. and Li, X. (2022) Floor Failure Characteristics of Thick Coal Seam Mining above Confined Aquifer. *Mining, Metallurgy & Exploration*, **39**, 1553-1562. https://doi.org/10.1007/s42461-022-00623-y

[13] Zeng, Y., Lian, H., Du, X., Tan, X. and Liu, D. (2022) An Analog Model Study on

Water-Sand Mixture Inrush Mechanisms during the Mining of Shallow Coal Seams. *Mine Water and the Environment*, **41**, 428-436. https://doi.org/10.1007/s10230-022-00870-x

[14] Song, C., Hu, X., Chen, Z. and Huang, W. (2024) Study on Stress—Fluid Coupling of Coal Seam Floor Water Outburst Based on FLAC 3D Simulation. *Chemistry and Technology of Fuels and Oils*, **59**, 1304-1312. https://doi.org/10.1007/s10553-024-01648-3

[15] Zhang, Y. (2021) Mechanism of Water Inrush of a Deep Mining Floor Based on Coupled Mining Pressure and Confined Pressure. *Mine Water and the Environment*, **40**, 366-377. https://doi.org/10.1007/s10230-020-00743-1

[16] Zhu, X., Zhang, Q., Liang, M. and Zhang, W. (2025) Mining-induced Damage Evolution and Infiltration Failure in Deep Mudstone-Sandstone Interbedded Strata. *Results in Engineering*, **28**, Article ID: 107095. https://doi.org/10.1016/j.rineng.2025.107095

[17] Shao, J., Zhang, Q. and Zhang, W. (2024) Evolution of Mining-Induced Water Inrush Disaster from a Hidden Fault in Coal Seam Floor Based on a Coupled Stress-Seepage-Damage Model. *Geomechanics and Geophysics for Geo-Energy and Geo-Resources*, **10**, Article No. 78. https://doi.org/10.1007/s40948-024-00790-w

[18] Liu, C., Zhang, P., Ou, Y., Yao, D. and Tian, Y. (2022) Analytical Stress Analysis Method of Interbedded Coal and Rock Floor over Confined Water: A Study on Mining Failure Depth. *Journal of Applied Geophysics*, **204**, Article ID: 104720. https://doi.org/10.1016/j.jappgeo.2022.104720

[19] Li, S., Bian, K., Han, G., Liu, B., Chen, X., Sun, H., *et al.* (2023) Study on Water Inrush Warning Information of Coal Seam Floor Fault Structure. *Energy Exploration & Exploitation*, **41**, 973-993. https://doi.org/10.1177/01445987231155980

[20] Song, W. and Zhao, C. (2024) Influence Analysis of Strata Dip on the Failure Characteristics and Groundwater Outburst Risk of Coal Seam Floor. *Environmental Earth Sciences*, **83**, Article No. 488. https://doi.org/10.1007/s12665-024-11787-9